Institute of Space and Aeronautical Science, University of Tokyo
Report No. 532, September 1975

Viscous Flow Around a Rotationally Oscillating Circular Cylinder

By

Atsushi OKAJIMA*, Hiroyuki TAKATA** and Tsuyoshi ASANUMA

Summary: Aerodynamic characteristics of a circular cylinder either stationary or rotationally oscillating around its axis in uniform viscous flow are studied by numerical calculation and by experiment. The method and results of numerical solution of the Navier-Stokes equations by the finite difference analogue are presented as well as measurements for the lift and the drag forces acting on the cylinder made by towing test models in still fluid in a range of Reynolds number, $Re=40$ to 6100. Good agreement is obtained between the calculated results and the experimental ones at Reynolds numbers $Re=40$ and 80, concerning the steady and unsteady aerodynamic parameters, the phenomenon of the so-called synchronization and so on. It becomes clear from numerical calculation that there may be a close relationship between the time-variation of the flow pattern and that of the lift force on an oscillating cylinder. Also by experiment the influence of Reynolds number on the aerodynamic parametersand the phenomenon of synchronization are examined.

1. INTRODUCTION

A considerable amount of discussion is found in the literature, concerning the wind-induced oscillations of smoke-stacks, cables and other structural forms and also the aeroelastic oscillations experienced in engineering. Information about the fluctuating forces acting on a cylinder, however, is still of considerable practical interest in aeroelasticity as well as in the basic understanding of fluid mechanics.

This paper is concerned with the study of flows around both a stationary circular cylinder and a circular cylinder subjected to the forced rotational oscillation around its axis, by the methods of both numerical solution of the Navier-Stokes equations and experiment.

Many attempts to solve the Navier-Stokes equations have been made and reported already for steady flow around a circular cylinder by Thom (1933), Kawaguti (1953), Allen and Southwell (1955), Apelt (1961), Keller and Takami (1966), Dennis and Chang (1970) and so on, and for unsteady flow around the circular cylinder which starts impulsively, by Payne (1958), Kawaguti and Jain (1966), Son and Hanratty (1969), Hamielec and Raal (1969) and so on. Fromm and Harlow (1963) performed numerical calculation for flow

* Research Institute for Applied Mechanics, Kyushu University, Fukuoka, Japan
** Department of Aeronautics, University of Tokyo, Tokyo, Japan

around a plate of rectangular cross-section which is placed perpendicular to flow in a channel of finite width. They were successful in first showing by numerical calculation that the Karman vortex street is generated behind that plate. Recently, Thoman and Szewczyk (1969) and Jordan and Fromm (1972) studied the problem of the Karman vortex street development behind the stationary circular cylinder.

Based on these studies, we present a method of numerical solution of the Navier-Stokes equations which is suitable for the cases treated in this paper. This method is justfied by comparing the results with others for the case of the stationary circular cylinder. Then a series of calculations are carried out for a circular cylinder oscillating rotationally around its axis while subjected to uniform viscous flow. The numerical solution of the Navier-Stokes equations, however, can be executed only for the low range of Reynolds number and in the present study some calculations are carried out for a circular cylinder, both stationary and oscillating in the range of the Reynolds number $Re=20$ to 80.

In addition, some experiments for stationary and oscillating cylinders are carried out first to confirm the validity of the present method of numerical calculation and second to study the case of Reynolds number higher than can be covered by the numerical calculation.

Meanwhile, experimental studies have been made for a circular cylinder oscillating in a uniform flow. Bishop and Hassan (1964), Jones (1968), Griffin (1972) and some others measured the lift and drag forces, and the velocity of a circular cylinder made to oscillate in a direction perpendicular to the stream. It was found that the so-called synchronization phenomenon of the system of cylinder and wake occurs when a cylinder oscillates transversally in uniform flow within a certain limited range of the ratio of the imposed frequency of a cylinder to the Strouhal frequency of vortex shedding from a stationary cylinder, and that within this frequency range of synchronization the measured lift force suffer changes in amplitude and phase as the imposed frequency is varied, that is, the aerodynamic damping forces becomes nagative and the transversl oscillation of the cylinder may become unstable, in the lower part of the imposed frequency of the synchronization range. The mechanism of this phenomenon, however, seems to be obscure as yet. Such a synchronization phenomenon, meanwhile, be analogized to take place when a cylinder is forced to oscillate rotationally around its axis.

The first half of the present paper is concerned with the method and results of numerical calculation and the latter half describes the experiment and compares its results with the calculated ones about aerodynamic parameters of a cylinder which is stationary or oscillating rotationally around its axis.

2. Numerical Calculation

2-1. Basic equations and boundary conditions

We consider an unsteady two-dimensional flow of an incompressible viscous fluid around a circular cylinder which oscillates rotationally with the ratio of a peripheral velocity to a uniform velocity, $V_0(t)$ around its axis while subjected to uniform flow, the velocity of which U is taken to be a unity.

In treating the flow around the circular cylinder, we use the orthogonal coordinates (ξ, η) which are expressed as $\xi=\log r/a$, $\eta=\theta$ in terms of polar coordinates (r, θ), where a is the radius of the cylinder and taken to be a unity.

Eliminating the pressure by taking rotation of the Navier-Stokes equations, we obtain the familiar transport equation for the vorticity.

$$\frac{\partial\zeta}{\partial t}+\frac{q_\xi}{h}\frac{\partial\zeta}{\partial\xi}+\frac{q_\eta}{h}\frac{\partial\zeta}{\partial\eta}=\frac{\nu}{h^2}\left(\frac{\partial^2\zeta}{\partial\xi^2}+\frac{\partial^2\zeta}{\partial\eta^2}\right) \tag{1}$$

where q_ξ, q_η are the ξ and η-components of flow velocity, $h=e^\xi$ is the scale factor of this coordinate system, ζ is the vorticity defined as $\zeta=\mathrm{e}^{-\xi}(\partial q_\eta/\partial\xi+q_\eta-\partial q_\xi/\partial\eta)$, ν is kinematic coefficient of viscosity, and t is time.

Then in the terms of the stream function ψ, q_ξ and q_η are, respectively,

$$hq_\xi=\frac{\partial\psi}{\partial\eta}, \qquad hq_\eta=-\frac{\partial\psi}{\partial\xi}. \tag{2}$$

The vorticity ζ is given in the terms of the seream function ψ by

$$\frac{\partial^2\psi}{\partial\xi^2}+\frac{\partial^2\psi}{\partial\eta^2}=-h^2\zeta. \tag{3}$$

For the convenience of the numerical treatment, we divide the stream function ψ into the following two parts,

$$\psi=\psi_p+\tilde{\psi} \tag{4}$$

where ψ_p corresponds to the stream function of potential flow around the circular cylinder, ($\psi_p=2aU\sinh\xi\sin\eta$: U is the uniform velocity of free stream.) and $\tilde{\psi}$ is the deviation of actual flow from the potential flow ψ_p.

Thus the final forms of basic equations are given as follows:

$$\frac{\partial\zeta}{\partial t}+\frac{1}{h^2}\left[\frac{\partial(\psi_p+\tilde{\psi})}{\partial\eta}\frac{\partial\zeta}{\partial\xi}-\frac{\partial(\psi_p+\tilde{\psi})}{\partial\xi}\frac{\partial\zeta}{\partial\eta}\right]=\frac{\nu}{h^2}\left(\frac{\partial^2\zeta}{\delta\xi^2}+\frac{\partial^2\zeta}{\partial\eta^2}\right) \tag{5}$$

$$\frac{\partial^2\tilde{\psi}}{\partial\xi^2}+\frac{\partial^2\tilde{\psi}}{\partial\eta^2}=-h^2\zeta \tag{6}$$

Equations (5) and (6) are to be solved for $\tilde{\psi}$ and ζ under appropriate initial and boundary conditions.

The boundary condition to be satisfied on the surface of the circular

cylinder is that there is no cross flow through the surface and also no slip flow along it, or

$$\phi_0=0, \qquad \left(\frac{\partial\psi}{\delta\xi}\right)_0=-V_0 \tag{7}$$

where suffix 0 denotes the value on the surface of the cylinder and V_0 is the surface velocity given by $(V_m+\Delta V\sin 2\pi f_c t)$ where V_m is the steady component of the surface velocity, ΔV is the amplitude of the oscillatory velocity while the the uniform velocity is taken to be a unity and f_c is the frequency of oscillation.

To specify the problem completely the other boundary condition should be imposed upon the flow field infinitely far from the cylinder. This condition is that the velocity of flow asymptotically tends to the uniform velocity U of the free stream as the distance becomes infinite. Referring to the detailed examination of this boundary condition in the appendix, we use the following approximate boundary condition in the present calculation:

$$\tilde{\psi}_\infty=A\xi_\infty \qquad \zeta_\infty=0 \tag{8}$$

where suffix ∞ indicates the value on the outer edge of the computational domain and A is the value determined by the implicit process in the calculation.

2-2. Aerodynamic coefficients

Using the stream function ψ and the vorticity ζ, the aerodynamic coefficients of the circular cylinder can be given in the following manner, where we use the radius a of the circular cylinder and the velocity U of the free stream as units of length and velocity respectively. Further, the Reynolds number may be defined in the usual way as $Re=2aU/\nu$.

Then the coefficient of the pressure of the surface of a circular cylinder is obtained by

$$C_p(\eta)-C_p(\eta=0)=\frac{4}{Re}\int_0^\eta\left(\frac{\partial\zeta}{\partial\xi}\right)_0 d\eta-2\frac{\partial V_0}{\partial t}\eta. \tag{9}$$

The coefficient of the local viscous shear stress on the surface becomes

$$C_\tau(\eta)=\frac{4}{Re}(\zeta_0-2V_0). \tag{10}$$

The lift and drag forces exerted on a unit spanlength of the cylinder consist of two components due to pressure and viscous shear stress. The ones due to the pressure are

$$C_{LP}=-\frac{1}{2}\int_0^{2\pi}C_p(\eta)\sin\eta\, d\eta\,,$$

$$C_{DP}=-\frac{1}{2}\int_0^{2\pi}C_p(\eta)\cos\eta\, d\eta\,, \tag{11}$$

and the others due to the visccous shear stress are

$$C_{LS}=\frac{1}{2}\int_0^{2\pi} C_\tau(\eta)\cos\eta\, d\eta\,,$$

$$C_{DS}=-\frac{1}{2}\int_0^{2\pi} C_\tau(\eta)\sin\eta\, d\eta\,. \tag{12}$$

Then the coefficients of the resultant lift and drag forces are, respectively,

$$C_L=C_{LP}+C_{LS}\,,$$

$$C_D=C_{DP}+C_{DS}\,. \tag{13}$$

2-3. Numerical procedure

In the numerical calculation, the rapid changes of the stream function and the vorticity in the flow field near the surface of the cylinder make it necessary to use a rather small mesh size close to the surface, but in the field far from the cylinder the use of a rather large mesh size may be adequate. This gradation of mesh size is conveniently achieved by transforming the physical plane into the (ξ, η)-plane as already described. This plane is then divided into a finite discrete mesh of points (iS, jS) with a constant mesh size, S, the is, the circumference of the cylinder is cut into N equal parts, i.e. $S=2\pi/N$. Further, just outsider, where the radial gradient of flow velocity seems to be most abrupt, the radial mesh is further divided into two $(S/2)$, namely, the mesh spacing in the ξ- and η- directions is denoted by S_ξ and S, respectively, and we call, here, the case of $S_\xi=S(=2\pi/N)$ the standard mesh and the case of $S_\xi=S/2$ the fine mesh. This fine mesh is certainly desirable in view of both the accuracy of computation and the economy of computing time. For convenience all expressions of a finite difference in the following, however, are obtained in the field divided into the standard mesh (iS, jS).

A finite difference analogue is used to compute the vorticity $\zeta^{t+\Delta t}(i,j)$ at each discrete time $t+\Delta t$ from the known values of the stream function $\psi^t(i,j)$ and the vorticity $\zeta^t(i,j)$ at time t, for all intersections (i,j) of mesh lines except the points of the surface, by solving the vorticity equations. Namely, the term $\partial\zeta/\partial t$ in equation (5) is replaced by $(\zeta^{t+\Delta t}(i,j))-\zeta^t(i,j))/\Delta t$ and averages between the values as determines for time $t+\Delta t$ and for time t are used as the values of ψ and ζ in the rest of this equation. Thus, equation (5) is given in the finite difference expression as follows:

$$\frac{\zeta^{t+\Delta t}(i,j)-\zeta^t(i,j)}{\Delta t}=\frac{2}{Re}\left(\frac{1}{2}\nabla^2\zeta^{t+\Delta t}(i,j)+\frac{1}{2}\nabla^2\zeta^t(i,j)\right)$$

$$+\frac{1}{16S^2h^2}(\zeta^{t+\Delta t}(i,j+1)+\zeta^t(i,j+1)-\zeta^{t+\Delta t}(i,j-1)-\zeta^t(i,j-1))$$

$$\times(\psi^{t+\Delta t}(i+1,j)+\psi^t(i+1,j)-\psi^{t+\Delta t}(i-1,j)-\psi^t(i-1,j))$$

$$-\frac{1}{16S^2h^2}(\zeta^{t+\Delta t}(i+1,j)+\zeta^t(i+1,j)-\zeta^{t+\Delta t}(i-1,j)-\zeta^t(i-1,j))$$

$$\times(\psi^{t+\Delta t}(i,j+1)+\psi^t(i,j+1)-\psi^{t+\Delta t}(i,j-1)-\psi^t(i,j-1)) \quad (14)$$

where $\psi^t(i,j)=\psi_p{}^t(i,j)+\tilde{\psi}^t(i,j)$

and

$$\nabla^2\zeta^t(i,j)=\frac{1}{S^2h^2}[\zeta^t(i,j+1)+\zeta^t(i,j-1)+\zeta^t(i+1,j)+\zeta^t(i-1,j)-4\zeta^t(i,j)].$$

The use of this kind of averaging process in the finite equation (14) should result in the implicit form.

Next, to solve equation (6) for $\tilde{\psi}(i,j)$ which corresponds to $\zeta(i,j)$, we employ the successive line over-relaxation method along concentric circular lines ξ=constant, sweeping from $\xi=0$ (on the surface of a cylinder) to $\xi=\xi_\infty$ (on the outer edge of the computational domain). The finite difference expression of equation (6) is

$$\tilde{\psi}^{K+1}(i,j)=\tilde{\psi}^K(i,j)+\omega[\tilde{\psi}^{K+1*}(i,j)-\tilde{\psi}^K(i,j)] \quad (15)$$

where

$$\tilde{\psi}^{K+1*}(i,j)$$

$$=\frac{1}{4}[\tilde{\psi}^K(i+1,j)+\tilde{\psi}^{K+1}(i-1,j)+\tilde{\psi}^{K+1*}(i,j+1)+\tilde{\psi}^{K+1*}(i,j-1)+S^2h^2\zeta(i,j)].$$

In equation (15), the superscript K indicates the value Kth iteration, and ω is a parameter known as an accelaration parameter which enhances convergence of this calculation. It optimum value is found to be *1.4* after several trials.

The boundary conditions used in this calculation are as follows, that is, on the surface of the cylinder ($i=1$),

$$\tilde{\psi}(1,j)=0, \qquad \zeta(1,j)=-\frac{2[\psi(2,j)-\psi(1,j)+V_0S]}{S^2} \quad (16)$$

and on the concentric circular boundary sufficiently far from the cylinder ($i=M$),

$$\tilde{\psi}(M,j)=A\cdot\xi_\infty, \qquad \zeta(M,j)=0 \quad (17)$$

where

$$A=-\frac{1}{SN}\sum_{j=1}^{N}(\tilde{\psi}(M,j)-\tilde{\psi}(M-1,j))$$

so, A is determined by the implicit process in the calculation.

3. Results of Numerical Calculation

3-1. Case of a stationary circular cylinder

It is desirable to test the accuracy of the present numerical method by

comparing the numerical results with the experimental ones previously obtained. In order to accomplish this, some calculations are first made for a stationary circular cylinder. The inviscid potential flow is used as the

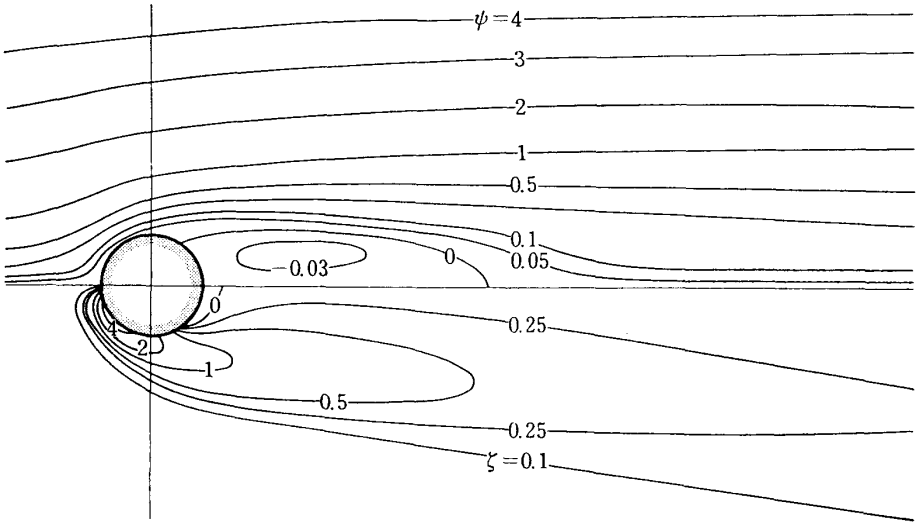

FIG. 1. Stream lines (the upper side) and equivorticity lines (the lower side) of a stationary circular cylinder at $Re=40$.

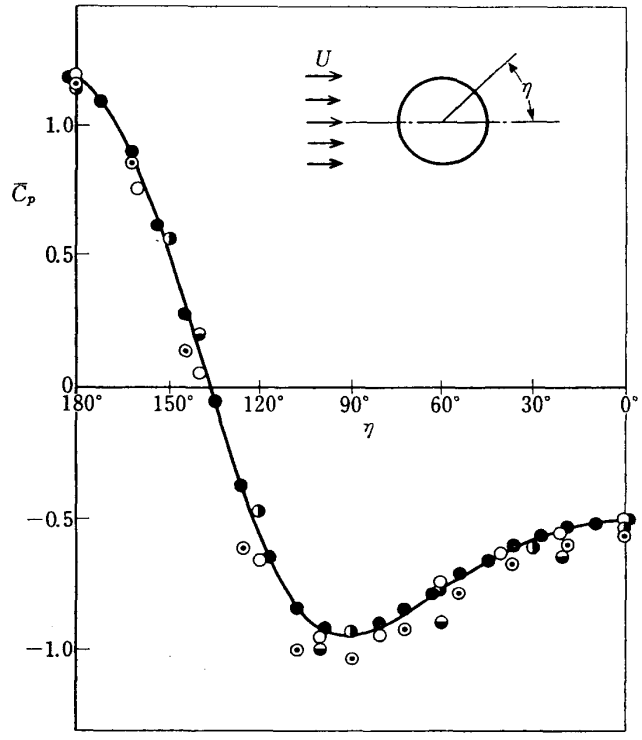

FIG. 2. Pressure distribution of the stationary circular cylinder at $Re=40$. Numerical solutions: -●-, present study; ◉, Apelt (1961); ◑, Kawaguti (1953). Experimental measurements: ○, Grove et al. (1960); ◒, Thom (1933) $Re=36$. The angle η is the degrees from backward stagnation point.

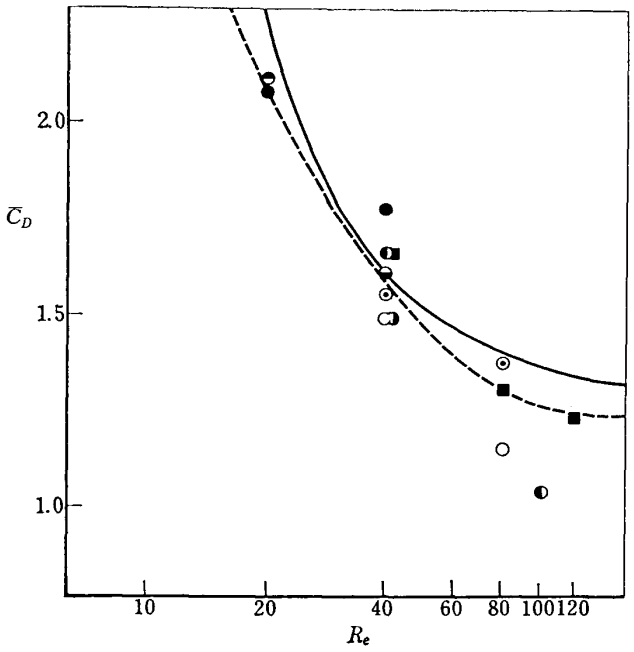

FIG. 3. Drag coefficients of the stationary circular cylinder. Present numerical solutions: ○, $N=40$ by fine mesh; ◉, $N=40$ by standard mesh; ●, $N=30$ by standard mesh. Other numerical solutions: ◑, Apelt (1961); ◒, Kawaguti (1953); ◐, Hirota and Miyakoda (1965); ◓, Thom (1933). Experimental measurements: ■, present study; ——, Relf and Simmons (1924); ----, Tritton (1959).

initial situation, which corresponds to the case that the cylinder starts impulsively from rest in a still fluid.

Figure 1 shows a typical example of calculated stream line and equivorticity line configurations around the stationary circular cylinder in uniform viscous flow at Reynolds number of $Re=40$. We can observe here that a pair of standing vortices are formed behind the cylinder, and that their size is in good agreement with calculated results by Apelt (1961) and others. The calculated pressure distribution on the surface of the cylinder agrees fairly well with the experimental results previously obtained, especiallythose of Grove et al. (1960), as shown in figure 2, where the angle η is measured from the backward stagnation point. In figure 3, the calculated drag force exerted on the cylinder is plotted as a non-dimensional expression together with some numerical and experimental results obtained by others in the range of $Re=$ 20 to 120. This figure shows it advisable to divide the flow domain into the finer net with an increase of Reynolds number. In this figure, also, we compare our calculated values with those of the others or with our and the other experimental values, considering the difference of flow patterns that in numerical calculation there are a pair of standing vortices, while in experiment the Karman vortex street alternately appears in the wake at Reynolds number over 40. It is confirmed that the standard mesh with the

parameter of calculation $N=30$ seems tobe adequate at $Re=20$, the fine mesh with $N=30$ or 40 at $Re=40$, and further at $Re=80$, the fine mesh with $N=40$ should be used at least. When the present calculation method is applied to the case of a rotationally oscillating circular cylinder in the following section, the standard mesh or the fine mesh with $N=40$ will be suitable for $Re=40$, and the fine mesh with $N=40$ for $Re=80$, to account for the economy of compution, although such net work may not be perfect in the accuracy of the calculation.

3-2. Case of a rotationally oscillating circular cylinder

We carry out a series of the calculation of the flow around a circular cylinder subjected to the forced oscillation around its axis in a uniform viscous flow, with the non-dimensional driving frequency defined as $St_c=2af_c/U$, f_c denoting the driving frequency, and with the ratio of the amplitude of peripheral velocity to uniform velocity, ΔV. From the results of calculation, in the range of the amplitude of oscillatory velocity / uniform velocity ratio, $\Delta V=0.2$ to 1.0, the magnitude of fluctuating lift force acting on the circular cylinder seems to be essentially proportional to ΔV, and its phase does not show a significant change. So, for the sake of convenience, the calculated results for only the case of $\Delta V=0.2$ will be presented in the following discussion.

Figure 4a shows the stream line configurations around a steadily rotating cylinder with a constant peripheral velocity $V_0=0.2$ for Reynolds number $Re=40$ at the time 52 and 60, which are elapsed after the abrupt start of steady rotation in a uniform flow and reduced into the dimensionless form by the ratio of a uniform velocity to a radius of the cylinder. We can clearly see a Karman vortex street being generated behind the cylinder in this figure. In general, a Karman vortex street cannot be generated behind the stationary cylinder at $Re=40$, as shown by Fromm and Harlow (1963). In this case, however, the shedding of the vortex street may be prompted by an unsymmetrical flow field due to the rotation of the cylinder. Therefore, as in figure 4b, a fluctuation of lift force exerted on the cylinder is caused by the generation of the Karman vortex street with the Strouhal frequency $St_k=0.11$ defined as $St_k=2af_k/U$, f_k denoting the frequencyof the Karman vortex street detected by the fluctuation of the lift force. In this figure, the wave forms of lift force are apparently composed of the mean value $\overline{C}_L$ of lift force due to the steady rotation and the component of fluctuation due to the Karman vortex street; C_{LP} and C_{LS} are the components of lift force due to pressure and viscous shear stress, respecively, and C_L is the resultant lift force.

Figure 5a shows the stream line configurations around a rotationally oscillating cylinder at the time $t=48$ and 56, the interval between which is nearly a half period of the imposed oscillation. The patterns of the vortex street at both times are almost upside-down in shape, each other so that the vortex street arrangement is found to change with the driving frequency $St_c=0.1$. Further, in figure 5b, we can see that the fluctuating lift force

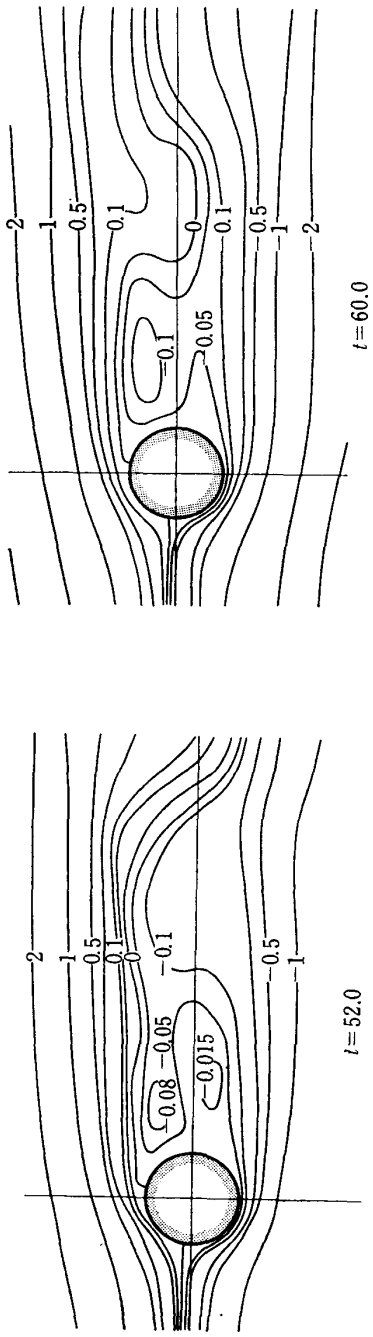

(a) Stream lines

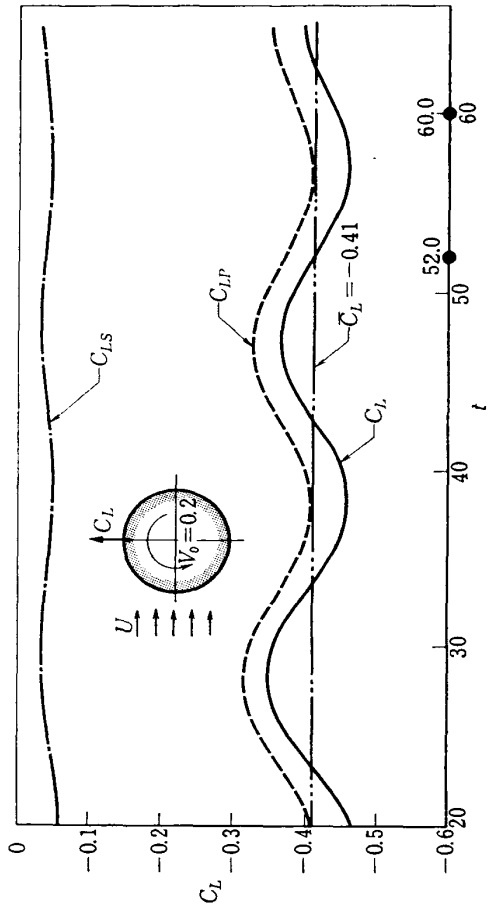

(b) Lift Force

FIG. 4. Stream lines and lift force of the steady rotating circular cylinder at $Re=40$ and $\Delta V=0.2$. ·-·-·—, the the mean value of lift force.

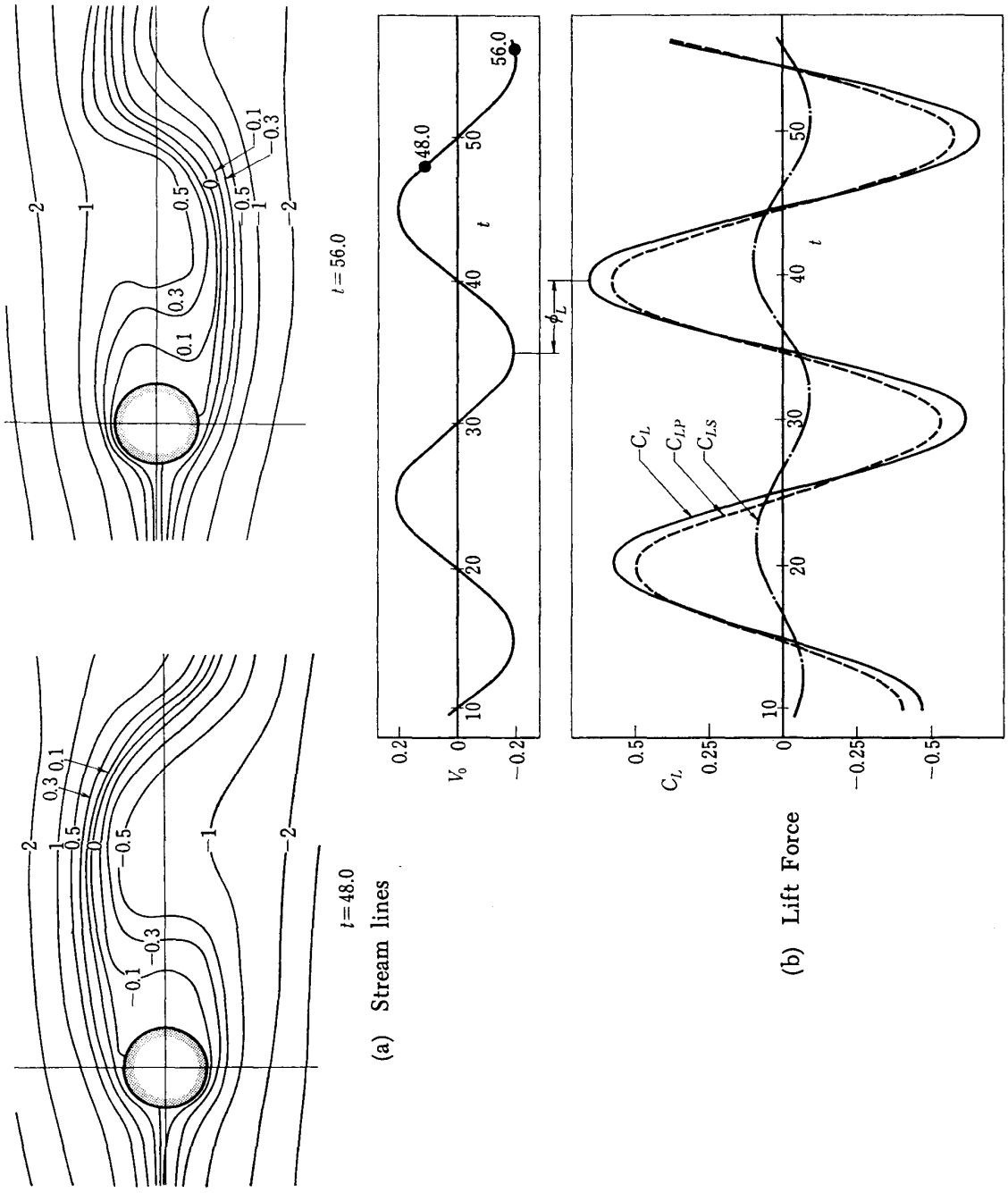

FIG. 5. Stream lines and lift force of the rotationally oscillating circular cylinder at $Re=40$, $St_c=0.1$ and $\Delta V=0.2$.

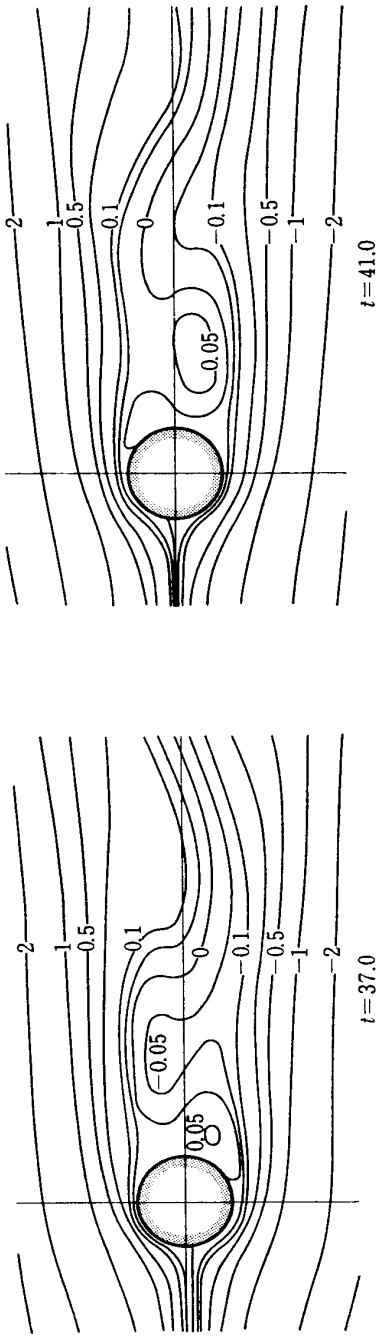

(a) Stream lines

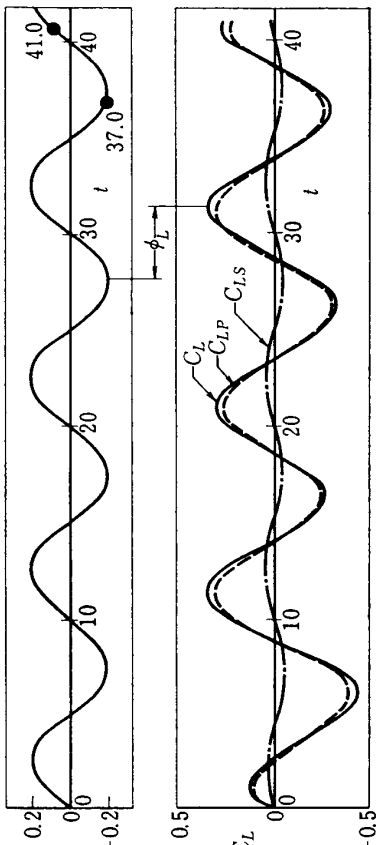

(b) Lift Force

FIG. 6. Stream lines and lift force of the rotationally oscillating circular cylinder at $Re=40$, $St=0.2$ and $\Delta V=0.2$.

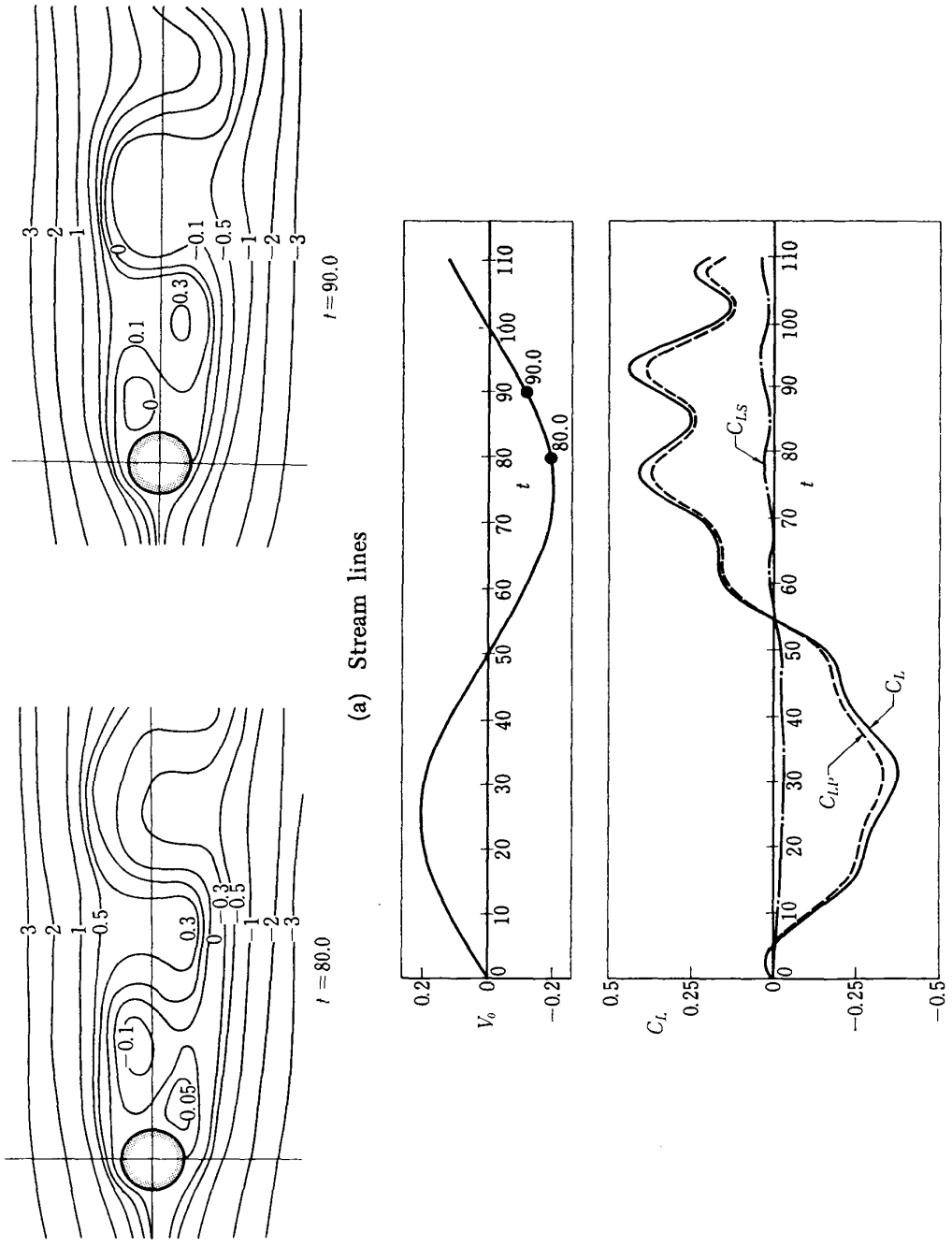

FIG. 7. Stream lines and lift force of the rotationally oscillating circular cylinder at $Re=80$, $St_c=0.02$ and $\Delta V=0.2$.

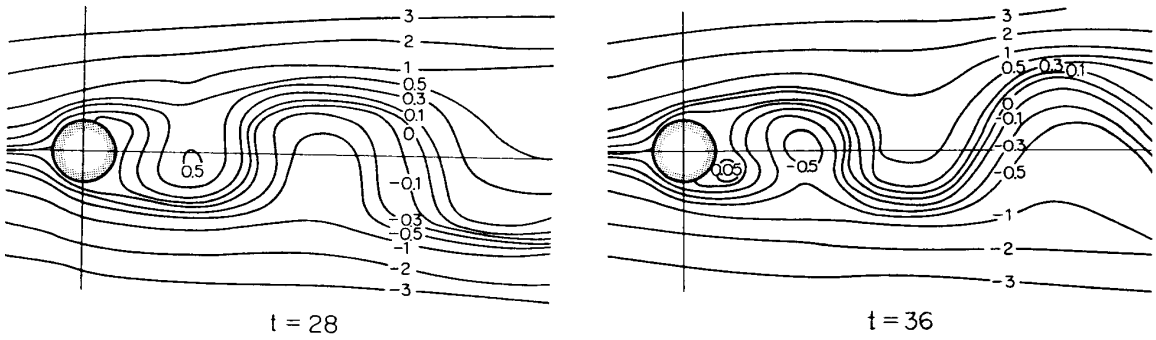

(a) Stream lines

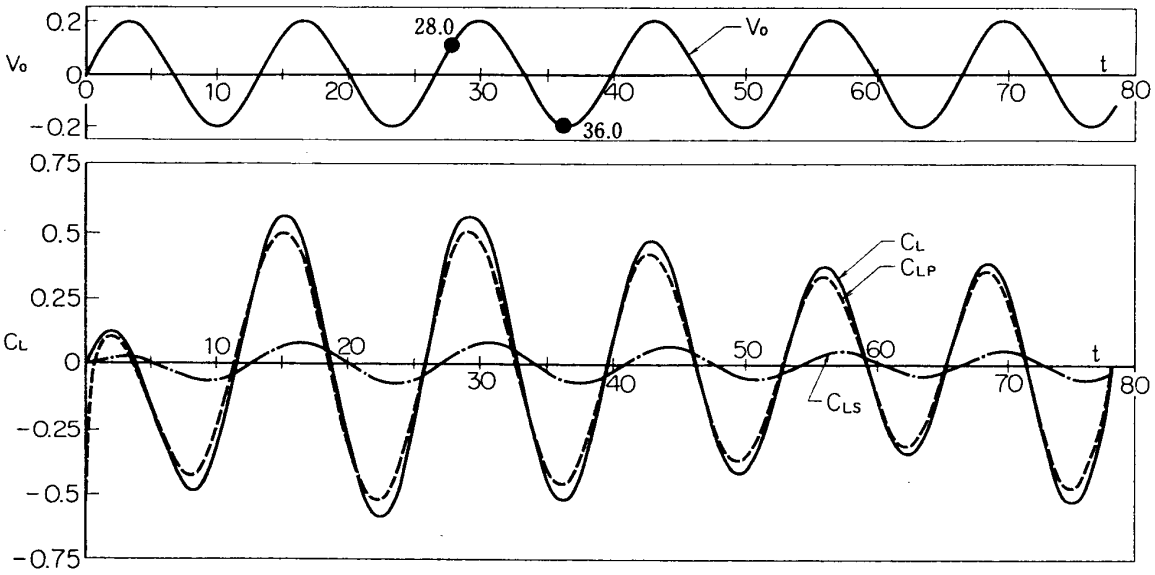

(b) Life Force

FIG. 8. Stream lines an lift force of the rotationally oscillating circular cylinder at $Re=80$, $St_c=0.15$ and $\Delta V=0.2$.

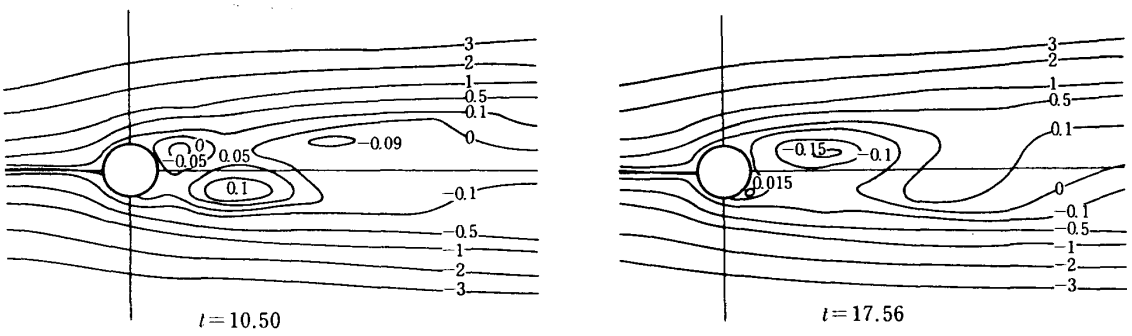

(a) Stream lines

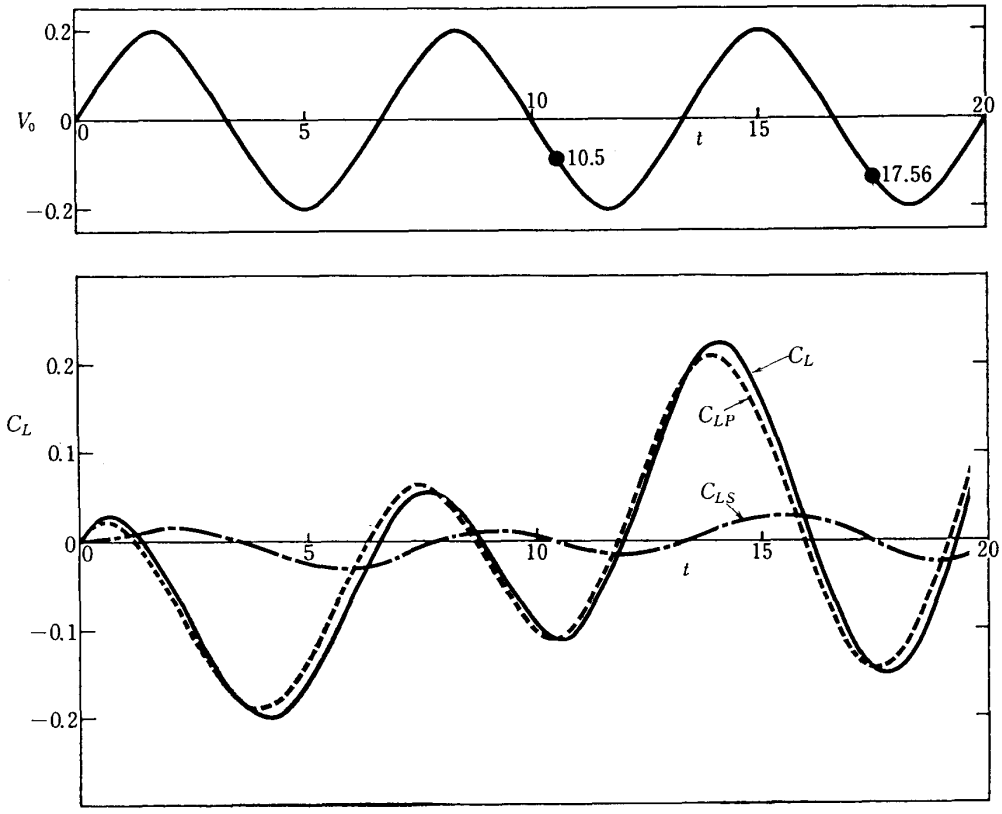

(b) Lift Force

FIG. 9. Stream lines and lift force of the rotationally oscillating circular cylinder at $Re=80$, $St_c=0.3$ and $\Delta V=0.2$.

exerted on the cylinder is fairly large with an amplitude of $|C_L| \simeq 0.55$, and it has a phase lag $\phi_L = -80°$ with respect to the motion of the cylinder or the quasi-steady lift force*.

With a still higher frequency $St_c = 0.2$, the vortex street is formed more distinctly behind the cylinder and the amplitude of the fluctuating lift force decreases to $|C_L| \simeq 0.22$, accompanied by a large lag $\phi_L = -125°$, as shown in figure 6.

Next, we examine the cases of the higher Reynolds number, $Re = 80$, as shown in figures 7, 8 and 9.

Figure 7 shows the flow patterns and the time-variation of the lift forces for the case of $Re = 80$ and the driving frequency $St_c = 0.02$ which is appreciably smaller than the Strouhal frequency St_k of the Karman vortex street. The stream line configurations at the time 80 and 90 shown in figure 7a, can be seen almost upside-down in shape, which implies the variation of the flow pattern with the period about 20 or $St_k \simeq 0.1$ in the expression of the Strouhal frequency. This Karman vortex street appearing behind the oscillating cylinder induces a fluctuation in the lift force, which is superimposed upon that due to the oscillation of the cylinder, as apparently shown in figure 7b.

When the driving frequency approaches the Strouhal frequency, i.e. $St_c = 0.15$, the flow patterns around a cylinder at the time $t = 36$ when the almost maximum lift force is exerted on the cylinder, and at the time $t = 28$, that is, about a half period of the forced oscillation before, are shown in figure 8a. The two flow configurations of the vortex street are also reverse in shape, so that the flow pattern is found to change with the same frequency as the imposed frequency $St_c = 0.15$. These facts imply that the system of the cylinder and the wake oscillates at the imposed frequency of the cylinder. In figure 8b, the lift force is fluctuating with the imposed frequency St_c without the Strouhal frequency, that is the two sets of lift forces induced by the Karman vortex street and the forced oscillation of the cylinder become synchronized. This amplitude, however, is not always constant over several periods, so the average of the amplitudes is about $|C_L| \simeq 0.4$ and its phase difference from the oscillation of the cylinder is $\phi_L = -100°$ lagging. Further, figure 9 is the case of the frequency of the cylinder greater than the Strouhal frequency of the Karman vortex street, i.e. $St_c = 0.3$. This figure shows the flow patterns at the time 10.50 and 17.56, the interval between which is about one period of the cylinder oscillation. By comparison of the two flow patterns in this figure, it is clear that the flow patterns are rather almost up-side down in shape at a short distance from the cylinder, although only the flow pattern near the cylinder is similar in shape each other. The prominent frequency of the fluctuating velocity in the field far

* When the cylinder oscillates rotationally with very low frequency, the force which is exerted on it by the Magnus effect may be assumed to be proportional to the oscillatory velocity with an opposite sign, i.e. $-V_0$. So, we will use the time variation of this quasi-steady force as the time basis.

from the cylinder is seen to be $St_k=0.13$ in the Strouhal frequency form, by examining the time variation of the fluctuating velocity in this field. Consequently, it is concluded that the field fluctuating with the frequency of the cylinder oscillation is restricted within the close vicinity of the cylinder and that the Karman vortex street can be observed in the wake far from the cylinder oscillating with the fast frequency, $St_c=0.3$. However, it is noteworthy that in the wave forms of the lift force in figure 9b, the component of the fluctuation induced by such Karman vortex street in wake being slightly detected, the lift force consists most of the component due to the fluctuating field with the imposed frequency St_c found only near the cylinder.

The variations of the amplitude and the phase-lag of the fluctuating lift force at $Re=40$ and 80 are summarized against the imposed frequency in figure 10. In this figure, the double amplitude of the superimposed lift forces by the Karman vortex street is represented by the arrow, and within the range of the so-called synchronization phenomenon, it seems reasonable for the amplitude of the lift force to reach a maximum value while accompanied by a large phase lag.

Each of the flow configurations at the time $t=48.0$ ($St_c=0.1$, $Re=40$), $t=37.0$ ($St_c=0.2$, $Re=40$) and $t=36.0$ ($St_c=0.15$, $Re=80$) as already shown in figure 5a, 6a, and 8a, respectively, is the pattern when the cylinder is experiencing almost a downward maximum value of the lift force. All of

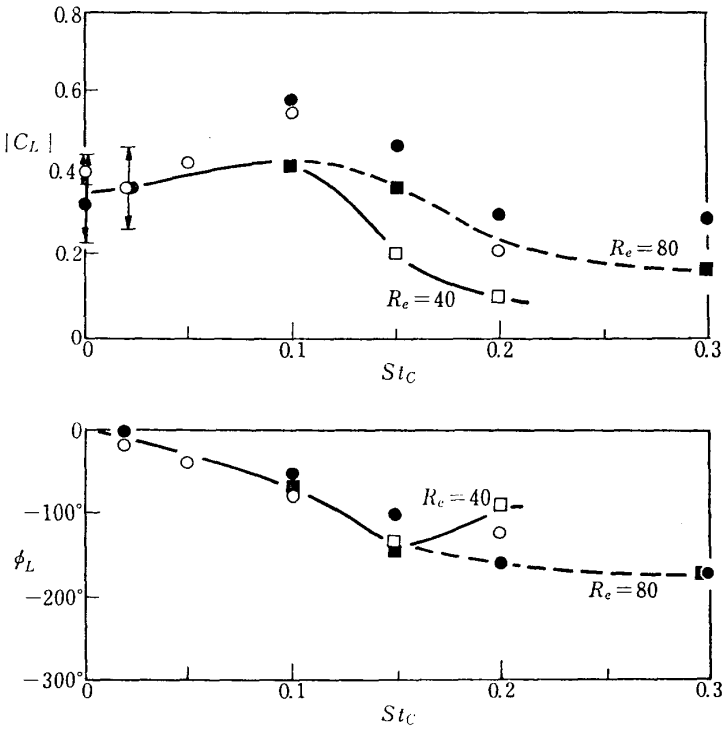

FIG. 10. The amplitudes and phases of lift force of the rotationally oscillating circular cylinder. By fine mesh: —□—, $Re=40$; --■--, $Re=80$. By standard mesh: ○, $Re=40$; ●, $Re=80$.

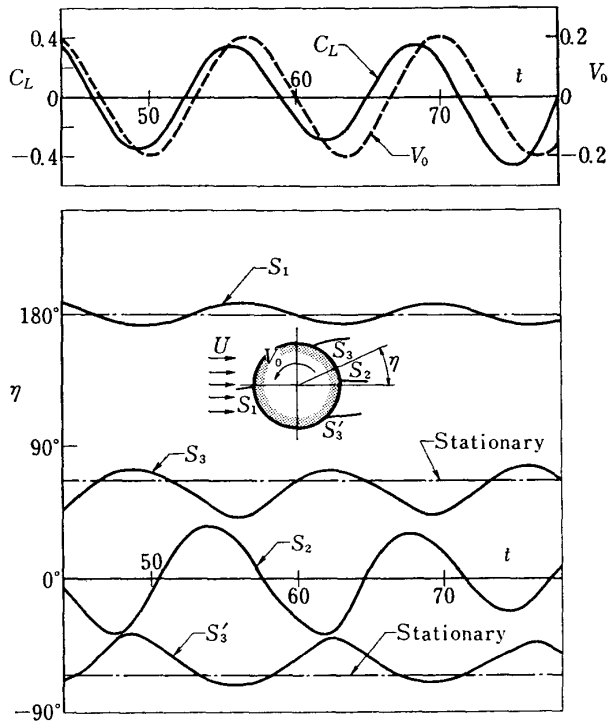

FIG. 11. The behaviours of the points S_1, S_2, S_3 and $S_{3'}$ where the shear stress vanishes for the rotationally oscillating circular cylinder at $Re=80$ and $St_c=0.15$. ——, the location for the stationary cylinder.

these figures are similar in shape where a vortex attached on the lower surface of the oscillating cylinder is growing to the largest size, and the same is true of the flow around the transversally oscillating cylinder numerically obtained by Okajima (1974). Therefore, the phase lagging of the variation of the lift force as summarized in figure 10 is clearly seen to agree with that of the change of the configuration of the vortex street in each case. We consider the behaviour of the flow near the surface of the cylinder, examining the movement of the points where the viscous shear stress vanishes on the surface, which correspond to the points of the flow stagnation and separation staying at the fixed points in the steady flow. As shown in figure 11 ($Re=80$, $St_c=0.15$), these points S_1, S_2, S_3 and $S_{3'}$ are seen to move with periodicity, and their frequencies are all the same as the imposed frequency St_c. At the time $t=55.5$ or 68.3 in this figure, the distance between the points S_2 and S_3 becomes minimum and that between S_2 and $S_{3'}$ is maximum, and in such a state, the cylinder is seen to be experiencing a maximum value of the lift force by reference to the time-variation of the lift force shown in figure 8b. This implies a close correlations between the movement of these points and the variation of the lift force.

4. Experimental Apparatus

The purpose of the present experiment is to measure the fluctuating lift and drag forces acting a circular cylinder subjected to the forced rotational oscillation around its axis with the specified amplitude and frequency. This is done not only to confirm the validity of the method of numerical calculation discussed in the previous section, but also to afford some information on such problem for higher Reynolds number.

So, we constructed an apparatus as shown in figure 12. By towing a test cylinder in a still liquid, either water or oil, of a tank, the uniformity of the velocity distribution in the spanwise direction of cylinder is sufficiently good except at its ends, and a low level of disturbance in flow can be expected. The test cylinder is made of hollow plastics as light as possible in weight in order to make measurement accurate.

4-1. Tank and carriage for measurement

As shown in figure 12, water or oil is in takn (1), which is 0.7m wide, 0.4m deep and about 10m long, and a carriage (3) with test cylinder (5) slides on tracks (2) by towing ropes (4) which are wound on a drum driven by an electric variable-speed motor. The test cylinder is hung vertically down from the carriage and is forced to oscillate rotationally around its axis with arbitrary frequency and amplitude by an oscillator mounted on the carriage. This oscillator consists of an electric variable-speed motor (6) which forces the test cylinder to oscillate around its axis through a gear

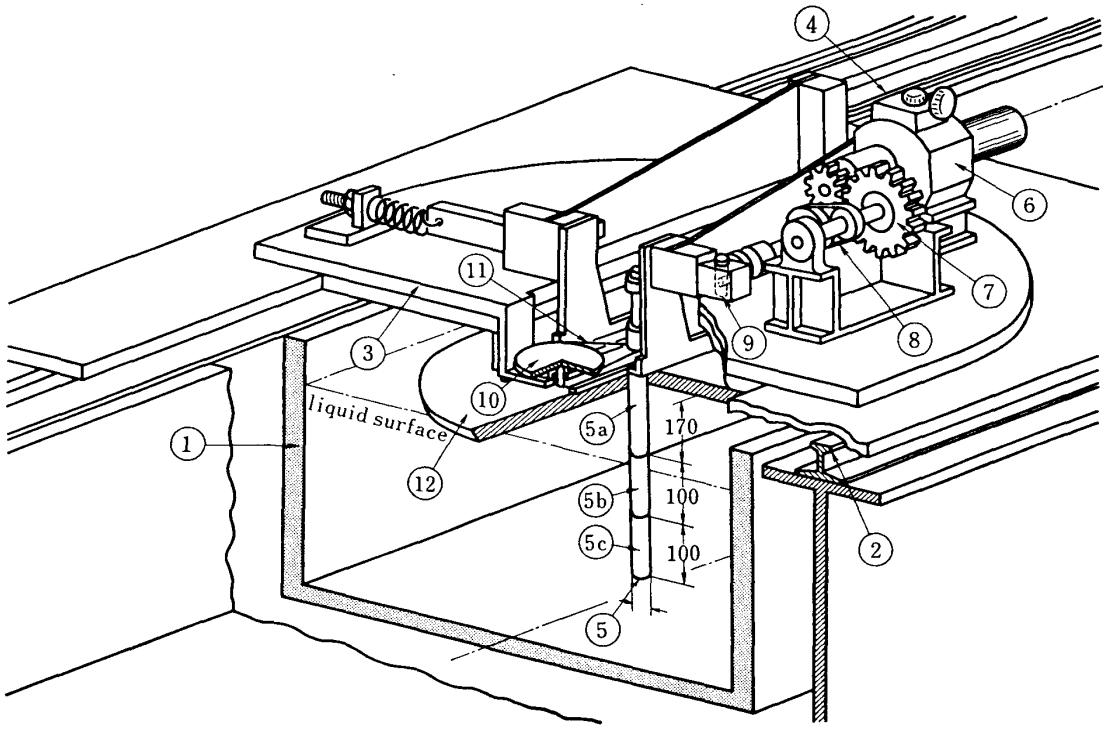

Fig. 12. Experimental apparatus.

train (7), a synchro-belt (8), a crank wheel and a scotch yoke mechanism (9), a driving wheel (10), a driving wire (11), and the test cylinder, in order of mention.

Many different kinds of experimental condition can be obtained by the following means. The Reynolds number may be changed by varying the towing speed between 5 cm/sec to 50 cm/sec or by exchanging water and oil as fluid substance, the oscillatory amplitude of the test cylinder by the selection of different crank wheels or driving wheels, and the oscillatory frequency by changing the speed of the oscillator motor. The available Reynolds numbers are thus about $Re=40$ to 160 for oil and $Re=3000$ to 6000 for water.

Since the present experiment is carried out by towing the test cylinder in still liquid with free surface, it is desirable to reduce the effects of surface wave and end-clearance as much as possible. For this reason a circular plastic disc (12) (diameter 500 mm) is mounted at the top of the test cylinder just touching the free surface of the liquid, and all of the measurements are made on the central part (5b) of the test cylinder, as described in the following section.

4-2. Test cylinder

The circular cylinder (5) is 30 mm in diameter and 370 mm in span-length, and divided into three sections (5a, 5b, 5c) in the spanwise direction, only the central one (5b) of which is used for the measurements so as not to suffer from the effects of three dimensional flow due to surface wave, end-clearance, and so on. The central section (5b) is 100 mm in span-length, made hollow to reduce its inertia as far as possible, and suspended from the upper dummy cylinder (5a) by two parallel leaf springs on which four strain gauges forming a Wheatstone bridge are mounted so as to be sensitive only to the component of the external force normal to these springs. The natural frequency of the central test cylinder suspended by the leaf springs is estimated to be over 20 Hz in water. The present experiment is conducted in a range of imposed frequency of the cylinder of less 2 Hz. Thus there shoud be no difficulty due to the above-mentioned natural frequency. The upper and the lower sections (5a, 5c) are 170 mm and 100 mm long in span and fastened to each other by two parallel connecting rods. The gaps between these three sections are adjusted to be 0.2 mm or less; they were also preliminarily checked to have no perceptible influence on the measurements.

The test cylinder is held fast to the supporting arms with two radial and one thrust bearings, and it is free to rotate around its axis when periodically forced by the oscillator. The supporting arms of the test cylinder are fixed to a turn-table on the carriage which makes it possible to measure the external force in any direction by turning the table and the test cylinder.

5. Experimental Results

In the present experiment, the two component forces the directions of

which are at right angles to each other are measured in separate runs, and the lift and drag component forces can be vectorially recomposed from these two components and reduced into the same non-dimensional forms of coefficients C_L and C_D as used in the numerical calculation.

5-1. Comparison between the experimental results and the calculated results at $Re=40$ and 80

For the drag coefficient $\overline{C}_D$ of the stationary circular cylinder, the comparison between the results of the present experiment and calculation were already presented in figure 3, in which it is clarified that they reasonably agree to each other and also with the results of the previous work (Relf and Simmons 1924, Tritton 1959).

Figure 13 shows typical records of the forces, F_1 and F_2, respectively, acting on a circular cylinder which is oscillating around its axis in uniform

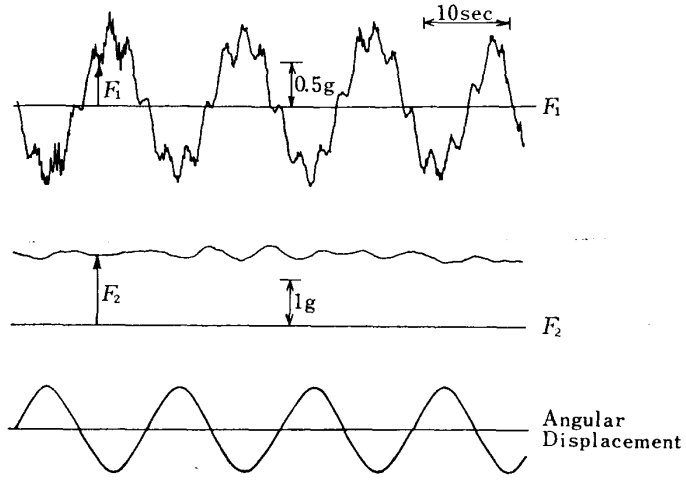

(a) $St_C=0.021$

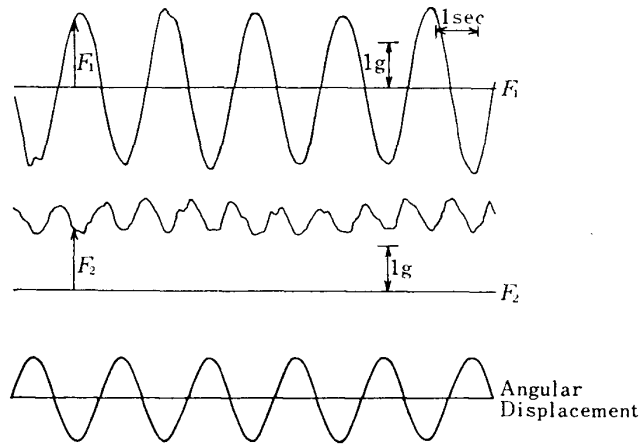

(b) $St_C=0.152$

FIG. 13. Typical records of forces acting on the rotationally oscillating circular cylinder at $Re=80$.
(a) $St_c=0.021$ and (b) $St_c=0.152$.

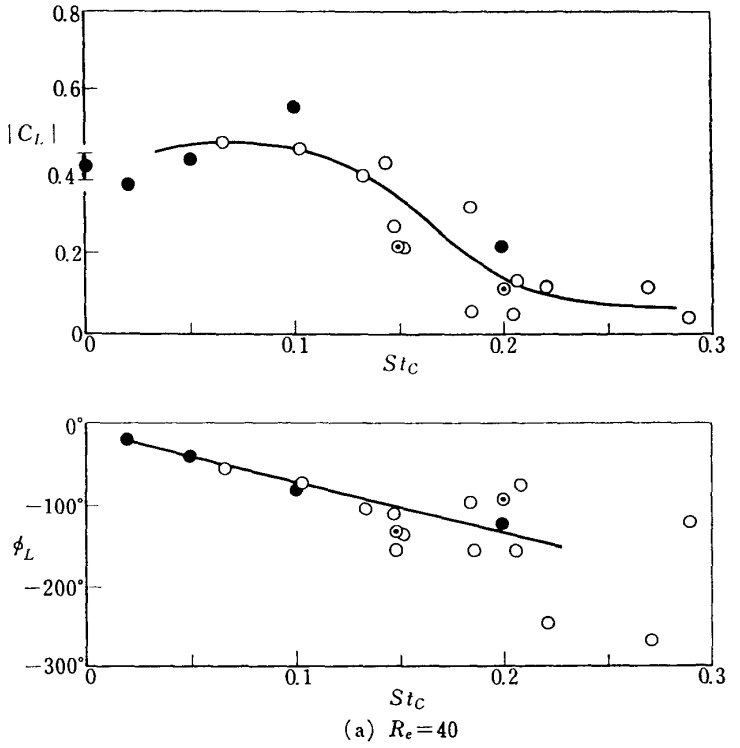

(a) $R_e=40$

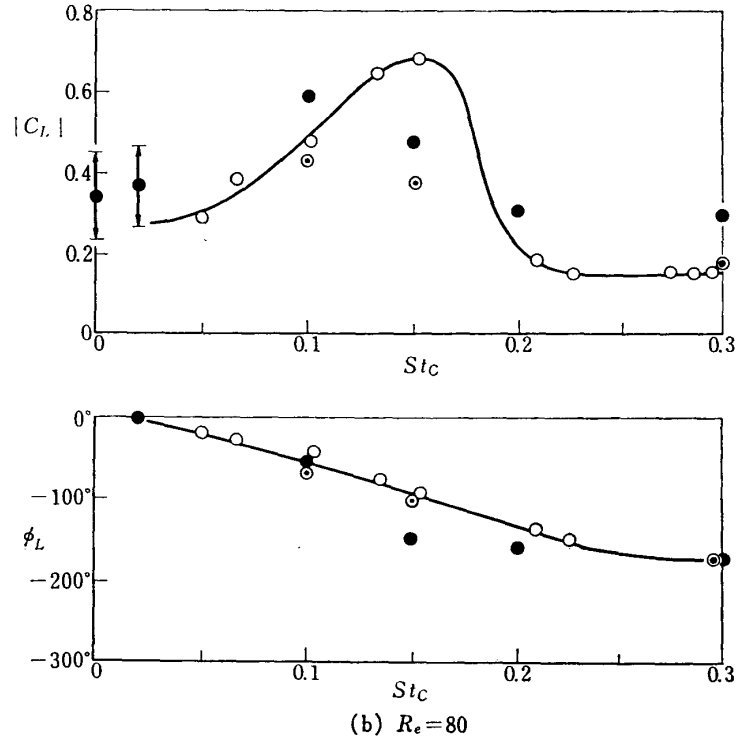

(b) $R_e=80$

FIG. 14. Calculated and experimental values of lift forces of the rotationally oscillating circular cylinder at $Re=40$, 80 and $\Delta V=0.2$. Numerical solutions: ●, by standard mesh, ◉, by fine mesh. Experimental measurements: —○—, lift force; ↕, the fluctuating components due to the Karman vortex street.

viscous flow in the case of $Re=80$. The directions of the forces F_1 and F_2 are set always to be at right angles. Since the amplitude of the angular displacement of oscillation is relatively small ($\Delta\theta=18°$) in this case, the variations of the forces F_1 and F_2 are nearly equal in shape but not in value to those of lift and drag forces, respectively. It is apparent in figure 13a ($St_c=0.021$) that the fluctuating force induced by Karman vortex street is superimposed on that due to the oscillation of the cylinder. This phenomenon corresponds to the calculated results that have been shown in figure 7, provided the driving frequency St_c of the cylinder is appreciably different from the Strouhal frequency St_k of the Karman vortex street ((a) $St_c=0.021$). However, when the driving frequency St_c approaches the Strouhal frequency St_k ((b) $St_c=0.152$), so-called synchronization phenomenon occurs, and the force F_1 oscillates at the imposed frequency and its amplitude becomes large. When St_c is greater than St_k, the force gets smaller and irregular.

In figure 14, the amplitude $|C_L|$ and phase angle ϕ_L of fluctuating lift forces are summarized and compared with the results of numerical calculation at $Re=40$ and 80. This figure shows that the experimental results coincide quite well with the calculated ones, not only in shape but also in

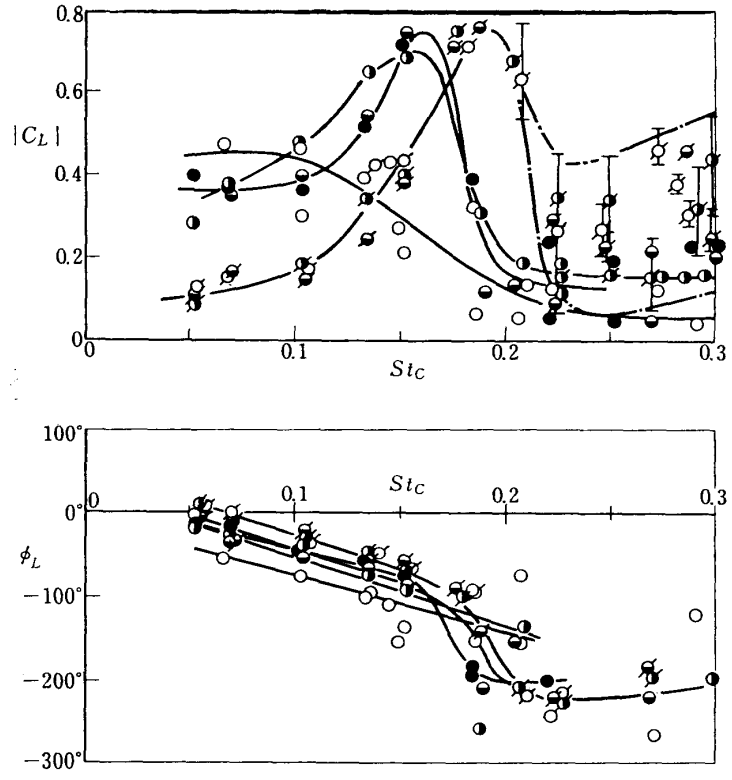

FIG. 15. The amplitudes and phases of the fluctuating lift forces of the rotationary oscillating circular cylinder. Case of low Reynolds numbers in oil: ○, $Re=40$: ◑, $Re=80$; ◒, $Re=120$; ●, $Re=160$ and case of high Reynolds numbers in water: ⌀, $Re=3050$; ⌀, $Re=4560$; ⌀, $Re=6100$.

value, although the experimental values of the amplitude and the phase of lift forces are scattered in the case of $Re=40$. Also, in the range where the synchronization phenomenon occurs ($St_c=0.1$ to 0.15), the fluctuating lift forces take a maximum value of amplitude and their phases lag behind with an increase in driving frequency.

5-2. Experimental results at higher Reynolds numbers

As the Reynolds number increases up to $Re=6100$, the fluctuating lift force does not suffer a great change in both the amplitude and the phase, but the range of synchronization about the middle of which their magnitude reach a maximum, accompanied by a large phase lagging, moves slightly to the region of the higher frequency, as shown in figure 15; in the range of Reynolds number $Re=3050$ to 6100, each of amplitude $|C_L|$ and the phase ϕ_L is nearly on one curve between $St_c=0$ and 0.2. Therefore, the fluctuatuating lift force is found to be weakly dependent on Reynolds number. In the range of the imposed frequency over 0.2, the record of lift forces exhibits a beating wave form composed by both the fluctuation of lift forces induced

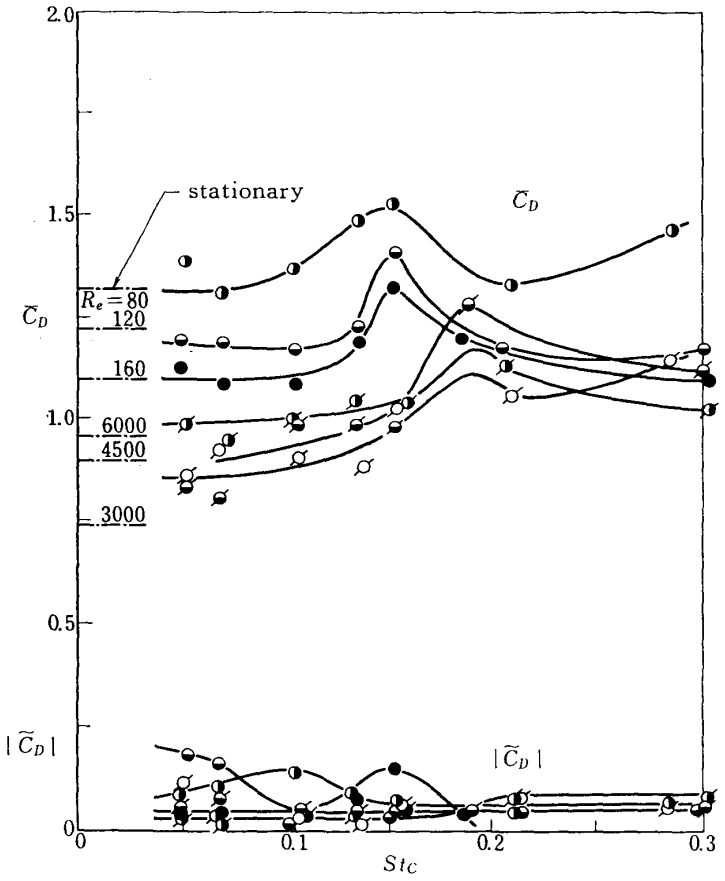

FIG. 16. Mean and fluctuating drag coefficients of the stationary and the rotationally oscillating circular cylinders. ◑, $Re=80$; ◒, $Re=120$; ●, $Re=160$; ⌀, $Re=3050$, ⌀, $Re=4560$; ⌀, $Re=6100$, ——·——, the case of stationary cylinder.

by Karman vortex with the Strouhal frequency St_k and the forces resulting from the motion of the cylinder with the frequency St_c. The amplitude of lift forces become so irregular and scattered that the difference between minimum and maximum values is shown by the width of vertical line in figure 15, to indicate the amount of scatter in measured values.

Figure 16 gives the magnitudes of the mean and the fluctuating drag forces, showing that the mean drag force has a maximum value within the range of synchronization and the fluctuating one is only about one-tenth as large as the former.

From the facts described above, it is apparent that the variations of the amplitude and phase of the lift forces and means drag forces against the imposed frequency in the synchronization range are found to be similar to that in the case of the transversal oscillation, which was previously studied by Bishop and Hassan (1964) and others.

6. Concluding Remarks

The aerodynamic characteristics of a circular cylinder subjected to a rotationary oscillation around its axis during uniform viscous flow were studied by both numerical calculation and experiment. Namely, we solved the Navier-Stokes equations and the continuity equation by finite difference method, and examined the detailed behaviours of the flow around both the stationary and rotationally oscillating circular cylinders. In addition, we carried out a series of experiment by towing the test cylinder submerged in still oil or water and measured the values of the unsteady lift and drag forces exerted on the stationary and the oscillating cylinders. There can be seen a fairly good agreement between the calculated results and the measured ones for the lift and drag forces acting on the stationary or the oscillating cylinder at Reynolds numbers $Re=40$ and 80. According to the numerical analysis, there may be close relationship between the time-variation of the flow pattern around the oscillating cylinder and the fluctuation of the lift force, that is, the phase lagging of the lift force of the cylinder oscillating with any frequency is clearly seen to agree with that of the time-variation of the configuration of the vortex street behind the cylinder. The unsteady lift and drag forces can be measured over the range of Reynolds numbers, $Re=40$ to 6100, and the phenomenon of the so-called synchronization is found to occur in a certain range of the ratio of the driving frequency to the Strouhal frequency, even when the circular cylinder undertakes the rational oscillation. The behaviour of the amplitude and phase of the lift force and mean drag force against the frequency in the synchronization range is similar to that in the case of the transversal oscillation of the circular cylinder.

Appendix: Boundary Conditions for the Field Infinitely far from the Cylinder

To solve a problem in an infinite field, it should be necessary to impose some of the boundary conditions on a field infinitely far from the cylinder. In a practical application of the computational problem including the infinite domain, however, the boundary conditions should be imposed on a far but finite boundary. The validity of the boundary conditions imposed on the far but finite boundary instead of the infinite one, as they relate to the boundary conditions used in this paper, will be examined here.

The deviation of stream function $\tilde{\phi}_\infty$ and the vorticity ζ_∞ in the far field, which are separated into two parts respectively, the steady ones, $\tilde{\phi}_{\infty s}$, $\zeta_{\infty s}$ and the unsteady ones, $\tilde{\phi}_{\infty u}$, $\zeta_{\infty u}$ will be investigated by the use of the linearized Oseen's equations which are presumably accurate in the field far from the cylinder. In the case of steady flow around the cylinder, Prof. Imai (1951) obtained asymptotic formulae of the steady parts $\tilde{\phi}_{\infty s}$ and $\zeta_{\infty s}$, as follows:

$$\tilde{\phi}_{\infty s}=\frac{\overline{C}_L^*}{2\pi}\cdot\log r_\infty-\frac{\overline{C}_D^*}{2}\left(\mathrm{erf}\,\alpha-\frac{\theta}{\pi}\right),\quad |\theta|<\pi \tag{A-1}$$

$$\zeta_{\infty s}=-\frac{\overline{C}_D^* Re}{4\sqrt{\pi}}\cdot\frac{\alpha}{r_\infty}\cdot e^{-\alpha^2}$$

where $\overline{C}_L^*$ and $\overline{C}_D^*$ are the steady components of lift and drag coefficients of the cylinder, $\alpha=\sqrt{(Re\cdot r_\infty/2)\sin(\theta/2)}$ and $\mathrm{erf}\,\alpha=\frac{2}{\sqrt{\pi}}\int_0^\alpha e^{-x^2}dx$. Next, we examine the asymptotic behaviours of the unsteady components $\tilde{\phi}_{\infty u}$ and $\zeta_{\infty u}$ by extending Imai's method and it may be easily shown that $\zeta_{\infty u}$ is estimated to be the order of e^{-r_∞} for large distance r_∞ under the influence of the oscillatory frequency and Reynolds number, and therefore that some terms of $\tilde{\phi}_{\infty u}$ which correspond to $\zeta_{\infty u}$ are also the order of e^{-r_∞}. While the term of $\tilde{\phi}_{\infty u}$ representing unsteady circulation around the cylinder should be omitted because of the single valuedness of pressure in flow field. However, in the actual computation, the value of distance r_∞ should be large but finite, so the values $\tilde{\phi}_{\infty u}$ and $\zeta_{\infty u}$ on the outer edge of the computational domain are given in asymptotic form as follows:

$$\tilde{\phi}_{\infty u}=A\xi_\infty,\qquad \zeta_{\infty u}=0 \tag{A-2}$$

where

$$A=-\frac{1}{SN}\sum_{j=1}^{N}(\tilde{\phi}(M,j)-\tilde{\phi}(M-1,j))\quad \text{at}\quad i=M\quad \text{(on the outer edge)}.$$

so, A is determined by the implicit process at eachtime step ofcalculation.

Now, we examine the magnitude of r_∞ which should be sufficiently large for the present calculation. We compare the calculated results of the drag coefficients, varying the distance r_∞, mesh point density and the value of

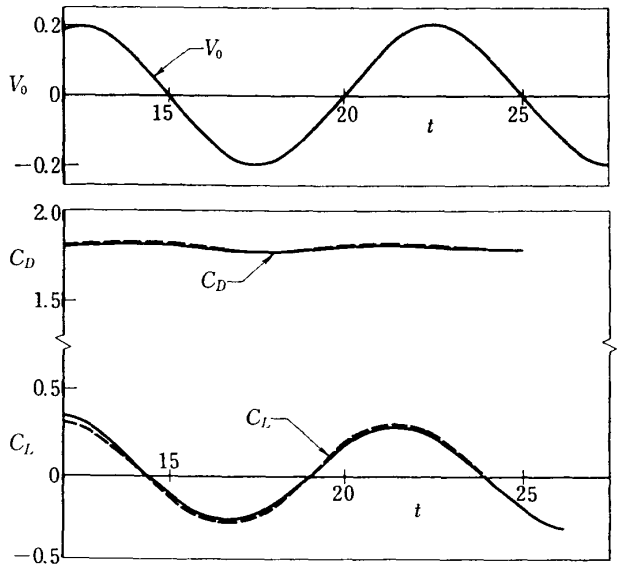

FIG. A-1. The comparison of the calculated results of the lift and drag forces for $r_\infty=111$ and $r_\infty=535$, at $Re=40$, $St_c=0.2$, $\Delta V=0.2$ and $\bar{C}_D{}^*=0$ in the equation (A-1).

$\bar{C}_D{}^*$ in equation (A-1), for the case of the stationary circular cylinder ($Re=40$). By the use of the standard mesh point density, we obtain $\bar{C}_D=1.86$, 1.80 and 1.56 as the steady drag coefficient value $\bar{C}_D$, taking $\bar{C}_D{}^*=0$ in equation (A-1) and $r_\infty=23$, $N=30$ (the mesh spacing is $S=2\pi/N$); $r_\infty=535$, $N=30$; $r_\infty=111$, $N=40$, respectively, and obtain $\bar{C}_D=1.72$, taking $\bar{C}_D{}^*=1.8$, $r_\infty=23$, $N=30$.

By the use of the fine mesh point density, $\bar{C}_D=1.49$ is obtained under the condititions of $\bar{C}_D{}^*=0$, $r_\infty=111$, $N=40$. There seem to be some discrepancies among their values. However these discrepancies are such that it may be practically valid to take $\bar{C}_D{}^*=0$ in equation (A-1), if r_∞ is taken to be sufficiently large, e.g. $r_\infty>100$ and also the field near the cylinder is divided into mesh point as fine as possible.

When the circular cylinder is oscillating around its axis, a comparison is made between the calculated results of lift and drag forces for $r_\infty=111$ and 535 as shown in figure A-1, by substituting $\bar{C}_D{}^*=0$ in equation (A-1).

In this case we can hardly find a discrepancy between these results. Therefore, afther the preliminary examination, we take r_∞ larger than 100 and $\bar{C}_D{}^*=0$ in equation (A-1) for the great part of our calculation.

Department of Jet Propulsion
Institute of Space and Aeronautical Science
University of Tokyo
July 30, 1975.

References

Allen, D. N. de G. and Southwell, R. V., 1955 Quart. J. Mech. Appl. Math. 8, 129.
Apelt, C. J., 1961 A. R. C. R. & M. 3175.
Bishop, R. E. D. and Hassan, A. Y., 1964 Proc. Roy. Soc. A **277**, 51.
Dennis, S. C. R. and Chang G. Z., 1970 J. Fluid Mech. **42**, 471.
Delany, N. K. and Sorensen, N. E., 1953 NACA TN, 3038.
Fromm, J. E. and Harlow, F. H., 1963 Phys. Fluids, **6**, 975.
Griffin, O. M. and Votaw, C. W., 1972 J. Fluid Mech. **55**, 31.
Grove, A. S., Shair, F. H., Peterson, E. E. and Acrivos, A., 1960 J. Fluid Mech. **19**, 60.
Hamielec, A. E. and Raal, J. D., 1969 Phys. Fluids **12**, 11.
Hirota, I. and Miyakoda, K., 1965 J. Metreor. Soc. Japan, **43**, 30.
Imai, I., 1951 Proc. Roy. Soc. A **208**, 487.
Jones, G. W., 1968 ASME Paper, 68-FE-36.
Jordan, S. K. and Fromm, J. E., 1972 Phys. Fluids **15**, 3, 371.
Kawauuti, M., 1953 J. Phys. Soc. Japan, 8, 6, 747.
Kawaguti, M. and Jain, P., 1966 J. Phys. Soc. Japan, **21**, 10, 2055.
Keller, H. B. and Takami, H., 1966 In Numerical Solutions of Nonlinear Differential Equations. (Ed. D. Greenspan) Englewood Cliffs, N. J.; Prentice-Hall.
Okajima, A., 1974 3rd Symp. on the wind effects on structures (in Japanese).
Payne, R. B., 1958 J. Fluid Mech. **4**, 81.
Relf, E. F. and Simmons, L. F. G., 1924 A. R. C. R. & M. 917.
Son, J. S. and Hanratty, T. J., 1969 J. Fluid Mech. **35**, 2, 369.
Thom, A., 1933 Proc. Roy. Soc. A **141**, 651.
Thoman, D. C. and Szewczyk, A. A., 1969 Phys. Fluid Suppl. II, 12, II-76.
Tritton, D. J., 1959 J. Fluid Mech. **6**, 547.